# Representation Learning of Histopathology Images using Graph Neural Networks

Mohammed Adnan[1,2,*], Shivam Kalra[1,*], Hamid R. Tizhoosh[1,2]
[1]Kimia Lab, University of Waterloo, Canada
[2]Vector Institute, Canada
{m7adnan,shivam.kalra,tizhoosh}@uwaterloo.ca

## Abstract

*Representation learning for Whole Slide Images (WSIs) is pivotal in developing image-based systems to achieve higher precision in diagnostic pathology. We propose a two-stage framework for WSI representation learning. We sample relevant patches using a color-based method and use graph neural networks to learn relations among sampled patches to aggregate the image information into a single vector representation. We introduce attention via graph pooling to automatically infer patches with higher relevance. We demonstrate the performance of our approach for discriminating two sub-types of lung cancers, Lung Adenocarcinoma (LUAD) & Lung Squamous Cell Carcinoma (LUSC). We collected 1,026 lung cancer WSIs with the 40× magnification from The Cancer Genome Atlas (TCGA) dataset, the largest public repository of histopathology images and achieved state-of-the-art accuracy of 88.8% and AUC of 0.89 on lung cancer sub-type classification by extracting features from a pre-trained DenseNet model.*

## 1. Introduction

Large archives of digital scans in pathology are gradually becoming a reality. The amount of information stored in such archives is both impressive and overwhelming. However, there is no convenient provision to access this stored knowledge and make it available to pathologists for diagnostic, research, and educational purposes. This limitation is mainly due to the lack of techniques for representing WSIs. The characterization of WSIs offers various challenges in terms of image size, complexity and color, and definitiveness of diagnosis at the pathology level, also the sheer amount of effort required to annotate a large number of images. These challenges necessitate inquiry into more effective ways of representing WSIs.

The recent success of "deep learning" has opened promising horizons for digital pathology. This has motivated both AI experts and pathologists to work together in order to create novel diagnostic algorithms. This opportunity has become possible with the widespread adoption of *digital pathology*, which has increased the demand for effective and efficient analysis of Whole Slide Images (WSIs). Deep learning is at the forefront of computer vision, showcasing significant improvements over conventional methodologies on visual understanding. However, each WSI consist of billions of pixel and therefore, deep neural networks cannot process them. Most of the recent work analyzes WSIs at the patch level, which requires manual delineation from an expert. Therefore, the feasibility of such approaches is rather limited for larger archives of WSIs. Moreover, most of the time, labels are available for the entire WSI, and not for individual patches. To learn a representation of a WSI, it is, therefore, necessary to leverage the information present in all patches. Hence, multiple instance learning (MIL) is a promising approach for learning WSI representation.

MIL is a type of supervised learning approach which uses a set of instances known as a bag. Each bag has an associated label instead of individual instances. MIL is thus a natural candidate for learning WSI representation. We explore the application of graph neural networks for MIL. We propose a framework that models a WSI as a fully connected graph to extract its representation. The proposed method processes the entire WSI at the highest magnification level; it requires a single label of the WSI without any patch-level annotations. Furthermore, modeling WSIs as fully-connected graphs enhance the interpretability of the final representation. We treat each instance as a node of the graph to learn relations among nodes in an end-to-end fashion. Thus, our proposed method not only learns the representation for a given WSI but also models relations among different patches. We explore our method for classifying two subtypes of lung cancer, Lung Adenocarcinoma (LUAD) and Lung Squamous Cell Carcinoma (LUSC). LUAD and LUSC are the most prevalent subtypes

*Authors have contributed equally.

of lung cancer, and their distinction requires visual inspection by an experienced pathologist. In this study, we used WSIs from the largest publicly available dataset, The Cancer Genome Atlas (TCGA) [30], to train the model for lung cancer subtype classification. We propose a novel architecture using graph neural networks for learning WSI representation by modeling the relation among different patches in the form of the adjacency matrix. Our proposed method achieved an accuracy of 89% and 0.93 AUC. The contributions of the paper are 3-folds, i) a graph-based method for representation learning of WSIs, and ii) a novel adjacency learning layer for learning connections within nodes in an end-to-end manner, and iii) visualizing patches which are given higher importance by the network for the prediction.

The paper is structured as follows: Section 2 briefly covers the related work. Section 3 discusses Graph Convolution Neural Networks (GCNNs) and deep sets. Section 4 explains the approach, and experiments & results are reported in Section 5.

## 2. Related Work

With an increase in the workload of pathologists, there is a clear need to integrate CAD systems into pathology routines [21, 24, 23, 10]. Researchers in both image analysis and pathology fields have recognized the importance of quantitative image analysis by using machine learning (ML) techniques [10]. The continuous advancement of digital pathology scanners and their proliferation in clinics and laboratories have resulted in a substantial accumulation of histopathology images, justifying the increased demand for their analysis to improve the current state of diagnostic pathology [24, 21].

**Histopathology Image Representation.** To develop CAD systems for histopathology images (WSIs), it is crucial to transform WSIs into feature vectors that capture their diagnostic semantics. There are two main methods for characterizing WSIs [2]. The first method is called *sub-setting method*, which considers a small section of a large pathology image as an essential part such that the processing of a small subset substantially reduces processing time. A majority of research studies in the literature have used the *subsetting* method because of its speed and accuracy. However, this method requires expert knowledge and intervention to extract the proper subset. On the other hand, the *tiling method* segments images into smaller and controllable patches (i.e., tiles) and tries to process them against each other [11], which requires a more automated approach. The tiling method can benefit from MIL; for example, Ilse et al. [15] used MIL with attention to classify breast and colon cancer images.

Due to the recent success of artificial intelligence (AI) in computer vision applications, many researchers and physicians expect that AI would be able to assist physicians in many tasks in digital pathology. However, digital pathology images are difficult to use for training neural networks. A single WSI is a gigapixel file and exhibits high morphological heterogeneity and may as well as contain different artifacts. All in all, this impedes the common use of deep learning [6].

**Multiple Instance Learning (MIL).** MIL algorithms assign a class label to a set of instances rather than to individual instances. The individual instance labels are not necessarily important, depending on the type of algorithm and its underlying assumptions. [3]. Learning representation for histopathology images can be formulated as a MIL problem. Due to the intrinsic ambiguity and difficulty in obtaining human labeling, MIL approaches have their particular advantages in automatically exploiting the fine-grained information and reducing efforts of human annotations. Isle et al. used MIL for digital pathology and introduces a different variety of MIL pooling functions [16]. Sudarshan et al. used MIL for histopathological breast cancer image classification [26]. Permutation invariant operator for MIL was introduced by Tomczak et al. and successfully applied to digital pathology images [27]. Graph neural networks (GNNs) have been used for MIL applications because of their permutation invariant characteristics. Tu et al. showed that GNNs can be used for MIL, where each instance acts as a node in a graph [28]. Anand et al. proposed a GNN based approach to classify WSIs represented by graphs of its constituent cells [1].

## 3. Background

**Graph Representation.** A graph can be fully represented by its node list $V$ and adjacency matrix $\mathbf{A}$. Graphs can model many types of relations and processes in physical, biological, social, and information systems. A connection between two nodes $V_i$ and $V_j$ is represented using an edge weighted by $a_{ij}$.

**Graph Convolution Neural Networks (GCNNs).** GCNNs generalize the operation of convolution from grid data to graph data. A GCNN takes a graph as an input and transforms it into another graph as the output. Each feature node in the output graph is computed by aggregating features of the corresponding nodes and their neighboring nodes in the input graph. Like CNNs, GCNNs can stack multiple layers to extract high-level node representations. Depending upon the method for aggregating features, GCNNs can be divided into two categories, namely spectral-based and spatial-based. Spectral-based approaches define graph convolutions by introducing filters from the perspective of graph signal processing. Spectral convolutions are defined as the multiplication of a node signal by a kernel.

This is similar to the way convolutions operate on an image, where a pixel value is multiplied by a kernel value. Spatial-based approaches formulate graph convolutions as aggregating feature information from neighbors. Spatial graph convolution learns the aggregation function, which is permutation invariant to the ordering of the node.

**ChebNet.** It was introduced by Defferrard et al. [5]. Spectral convolutions on graphs are defined as the multiplication of a signal $x \in R^N$ (a scalar for every node) with a filter $g(\theta) = diag(\theta)$ parameterized by $\theta \in R^N$ in the Fourier domain, i.e.,

$$g_\theta \circledast x = U g_\theta U^T x,$$

where $U$ is the matrix of eigenvectors of the normalized graph Laplacian $L = I_N - D^{-\frac{1}{2}} A D^{-\frac{1}{2}}$. This equation is computationally expensive to calculate as multiplication with the eigenvector matrix U is $O(N^2)$. Hammond et al. [13] suggested that that $g_\theta$ can be well-approximated by a truncated expansion in terms of Chebyshev polynomials $T_k(x)$, i.e,

$$g_{\theta'}(\Lambda) \approx \sum_{k=0}^{K} \theta' T_k(\Lambda).$$

The kernels used in ChebNet are made of Chebyshev polynomials of the diagonal matrix of Laplacian eigenvalues. ChebNet uses kernel made of Chebyshev polynomials. Chebyshev polynomials are a type of orthogonal polynomials with properties that make them very good at tasks like approximating functions.

**GraphSAGE.** It was introduced by Hamilton et al. [12]. GraphSAGE learns aggregation functions that can induce the embedding of a new node given its features and neighborhood. This is called inductive learning. GraphSAGE is a framework for inductive representation learning on large graphs that can generate low-dimensional vector representations for nodes and is especially useful for graphs that have rich node attribute information. It is much faster to create embeddings for new nodes with GraphSAGE.

**Graph Pooling Layers.** Similar to CNNs, pooling layers in GNNs downsample node features by pooling operation. We experimented with Global Attention Pooling, Mean Pooling, Max Pooling, and Sum Pooling. Global Attention Pooling [22] was introduced by Li et al. and uses soft attention mechanism to decide which nodes are relevant to the current graph-level task and gives the pooled feature vector from all the nodes.

**Universal Approximator for Sets.** We use results from Deep Sets [32] to get the global context of the set of patches representing WSI. Zaheer et al. proved in [32] that any set can be approximated by $\rho \sum(\phi(x))$ where $\rho$ and $\phi$ are some function, and $x$ is the element in the set to be approximated.

## 4. Method

The proposed method for representing a WSI has two stages, i) sampling important patches and modeling them into a fully-connected graph, and ii) converting the fully-connected graph into a vector representation for classification or regression purposes. These two stages can be learned end-to-end in a single training loop. The major novelty of our method is the learning of the adjacency matrix that defines the connections within nodes. The overall proposed method is shown in Figure 1 and Figure 2. The method can be summarized as follows.

1. The important patches are sampled from a WSI using a color-based method described in [18]. A pre-trained CNN is used to extract features from all the sampled patches.

2. The given WSI is then modeled as a fully-connected graph. Each node is connected to every other node based on the adjacency matrix. The adjacency matrix is learned end-to-end using Adjacency Learning Layer.

3. The graph is then passed through a Graph Convolution Network followed by a graph pooling layer to produce the final vector representation for the given WSI.

The main advantage of the method is that it processes entire WSIs. The final vector representation of a WSI can be used for various tasks—classification (prediction cancer type), search (KNN search), or regression (tumor grading, survival prediction) and others.

**Patch Selection and Feature Extraction.** We used the method for patch selection proposed in [18]. Every WSI contains a bright background that generally contains irrelevant (non-tissue) pixel information. We removed non-tissue regions using color thresholds. Segmented tissue is then divided into patches. All patches are grouped into a pre-set number of categories (classes) via a clustering method. A portion of all clustered patches (e.g., 10%) are randomly selected within each class. Each patch obtained after patch selection is fed into a pre-trained DenseNet [14] for feature extraction. We further feed these features to trainable fully connected layers and obtain final feature vectors each of dimension 1024 representing patches.

**Graph Representation of WSI.** We propose a novel method for learning WSI representation using GCNNs. Each WSI is converted to a fully-connected graph, which has the following two components.

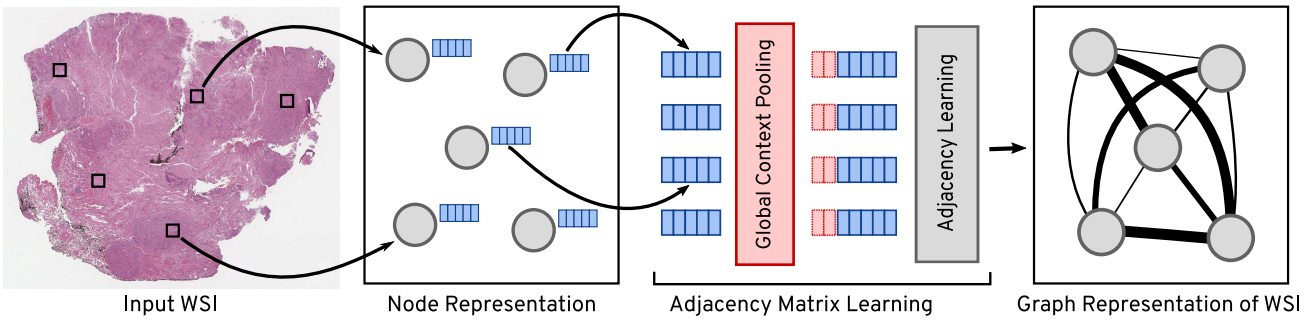


Figure 1: **Transforming a WSI to a fully-connected graph.** A WSI is represented as a graph with its nodes corresponding to distinct patches from the WSI. A node feature (a blue block beside each node) is extracted by feeding the associated patch through a deep network. A single context vector, summarizing the entire graph is computed by pooling all the node features. The context vector is concatenated with each node feature, subsequently fed into adjacent learning block. The adjacent learning block uses a series of dense layers and cross-correlation to calculate the adjacency matrix. The computed adjacency matrix is used to produce the final fully-connected graph. In the figure, the thickness of the edge connecting two nodes corresponds to the value in the adjacency matrix.

1. Nodes $V$: Each patch feature vector represents a node in the graph. The feature for each node is the same as the feature extracted for the corresponding patch.

2. Adjacency Matrix $\mathbf{A}$: Patch features are used to learn the $\mathbf{A}$ via adjacency learning layer.

**Adjacency Learning Layer.** Connections between nodes $V$ are expressed in the form of the adjacency matrix $\mathbf{A}$. Our model learns the adjacency matrix in an end-to-end fashion in contrast to the method proposed in [28] that thresholds the $\ell_2$ distance on pre-computed features. Our proposed method also uses global information about the patches while calculating the adjacency matrix. The idea behind using the global context is that connection between two same nodes/patches can differ for different WSIs; therefore, elements in the adjacency matrix should depend not only on the relation between two patches but also on the global context of all the patches.

1. Let $W$ be a WSI and $w_1, w_2, \ldots w_n$ be its patches. Each patch $w_i$ is passed through a feature extraction layer to obtain corresponding feature representation $x_i$.

2. We use the theorem by Zaheer et al. [32] to obtain the global context from the features $x_i$. Feature vectors from all patches in the given WSI are pooled using a pooling function $\phi$ to get the global context vector $c$. Mathematically,

$$c = \phi(x_1, x_2, \ldots, x_n). \tag{1}$$

   Zaheer et al. showed that such a function can be used as an universal set approximator.

3. The global context vector $c$ is then concatenated to each feature vector $x_i$ to obtain concatenated feature vector $x_i'$ which is passed through MLP layers to obtain new feature vector $x_i^* \cdot x_i^*$ are the new features that contain information about the patch as well as the global context.

4. Features $x_i^*$ are stacked together to form a feature matrix $\mathbf{X}^*$ and passed through a cross-correlation layer to obtain adjacency matrix denoted by $\underset{n\times n}{\mathbf{A}}$ where each element $a_{ij}$ in $\mathbf{A}$ shows the degree of correlation between the patches $w_i$ and $w_j$. We use $a_{ij}$ to represent the edge weights between different nodes in the fully connected graph representation of a given WSI.

**Graph Convolution Layers.** Once we implemented the graph representation of the WSI, we experimented with two types of GCNN: ChebNets and GraphSAGE Convolution, which are spectral and spatial methods, respectively. Each hidden layer in GCNN models the interaction between nodes and transforms the feature into another feature space. Finally, we have a graph pooling layer that transforms node features into a single vector representation. Thus, a WSI can now be represented by a condensed vector, which can be further used to do other tasks such as classification, image retrieval, etc.

**General MIL Framework.** Our proposed method can be used in any MIL framework. The general algorithm for solving MIL problems is as follows:

1. Consider each instance as a node and its corresponding feature as the node features.

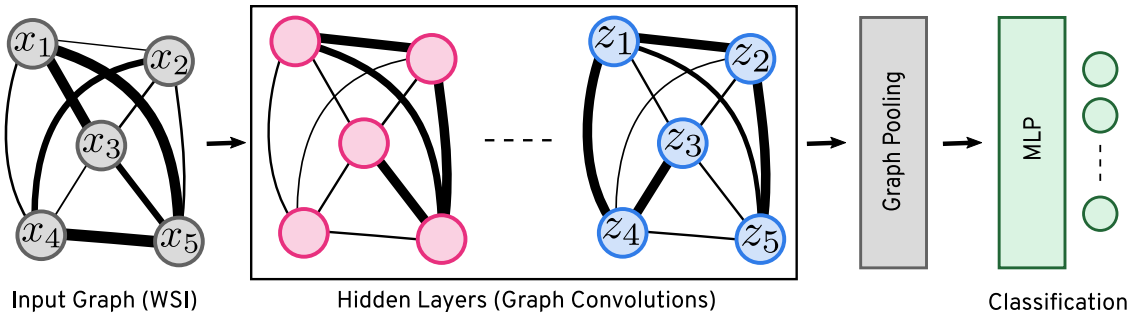


Figure 2: **Classification of a graph representing a WSI.** A fully connected graph representing a WSI is fed through a graph convolution layer to transform it into another fully-connected graph. After a series of transformations, the nodes of the final fully-connected graph are aggregated to a single condensed vector, which is fed to an MLP for classification purposes.

2. The global context of the bag of instances is learned to calculate the adjacency matrix **A**.

3. A fully connected graph is constructed with each instance as a node and $a_{ij}$ in $A$ representing the edge weight between $V_i$ and $V_j$.

4. Graph convolution network is used to learn the representation of the graph, which is passed through a graph pooling layer to get a single feature vector representing the bag of instances.

5. The single feature vector from the graph can be used for classification or other learning tasks.

## 5. Experiments

We evaluated the performance of our model on two datasets i) a popular benchmark dataset for MIL called MUSK1 [7], and ii) 1026 lung slides from TCGA dataset [11]. Our proposed method achieved a state-of-the-art accuracy of 92.6% on the MUSK1 dataset. We further used our model to discriminate between two sub-types of lung cancer—Lung Adenocarcinoma (LUAD) and Lung Squamous Cell Carcinoma (LUSC).

**MUSK1 Dataset.** It has 47 positive bags and 45 negative bags. Instances within a bag are different conformations of a molecule. The task is to predict whether new molecules will be musks or non-musks. We performed 10 fold cross-validation five times with different random seeds. We compared our approach with various other works in literature, as reported in Table 1. The miGraph [33] is based on kernel learning on graphs converted from the bag of instances. The latter two algorithms, MI-Net [29], and Attention-MIL [15], are based on DNN and use either pooling or attention mechanism to derive the bag embedding.

| Algorithm | Accuracy |
|---|---|
| mi-Graph [33] | 0.889 |
| MI-Net [29] | 0.887 |
| MI-Net with DS [29] | 0.894 |
| Attention-MIL [15] | 0.892 |
| Attention-MIL with gating [15] | 0.900 |
| Ming Tu et al. [28] | 0.917 |
| **Proposed Method** | **0.926** |

Table 1: Evaluation on MUSK1.

**LUAD vs LUSC Classification.** Lung Adenocarcinoma (LUAD) and Lung Squamous Cell Carcinoma (LUSC) are two main sub-types of non-small cell lung cancer (NSCLC) that account for 65-70% of all lung cancers [9]. Automated classification of these two main subtypes of NSCLC is a crucial step to build computerized decision support and triage systems.

We obtained 1,026 hematoxylin and eosin (H&E) stained permanent diagnostic WSIs from TCGA repository [11] encompassing LUAD and LUSC. We selected relevant patches from each WSI using a color-based patch selection algorithm described in [18, 19]. Furthermore, we extracted image features from these patches using DenseNet [14]. Now, each bag in this scenario is a set of features labeled as either LUAD or LUSC. We trained our model to classify bags as two cancer subtypes. The highest 5-fold classification AUC score achieved was 0.92, and the average AUC across all folds was 0.89. We performed cross-validation across different patients, i.e., training was performed using WSIs from a totally different set of patients than the testing. The results are reported in Table 2. We achieved state-of-the-art accuracy using the transfer learning scheme. In other words, we extracted patch features from an existing pre-trained network, and the feature extractor was not re-trained or fine-tuned during the training process. The Figure 5 shows the receiver operating curve (ROC) for one of the folds.

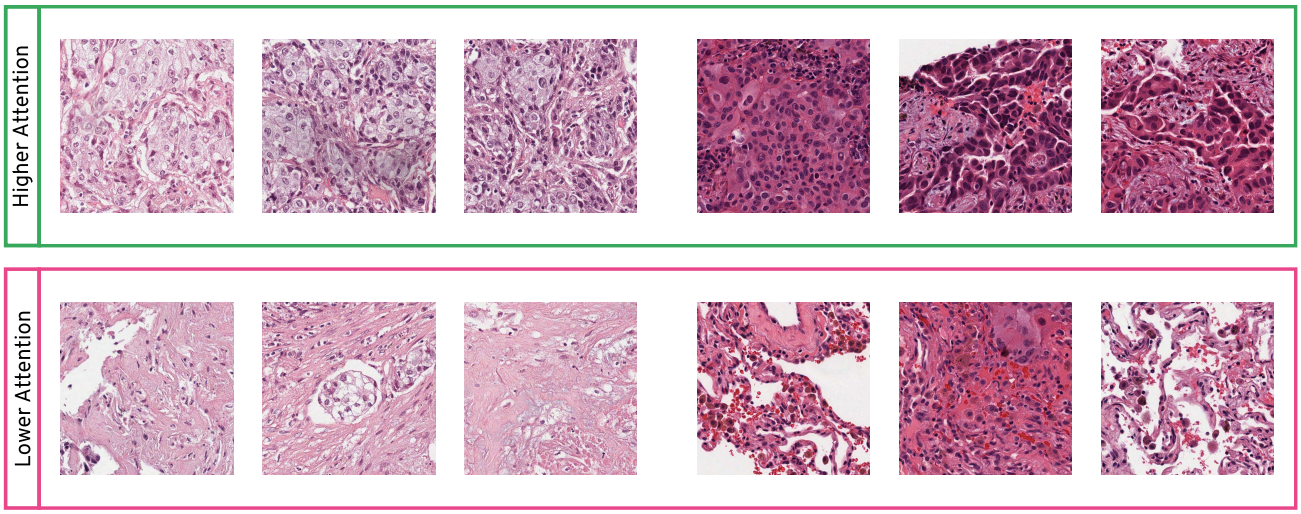


(a) Lung Squamous Cell Carcinoma (b) Lung Adenocarcinoma

Figure 3: Six patches from two WSIs diagnosed with LUSC and LUAD, respectively. The six patches are selected, such that the first three (top row) are highly "attended" by the network, whereas the last three (bottom row) least attended. The first patch in the upper row is the most attended patch (more important) and the first patch in the lower row in the least attended patch (less important).

| **Algorithm** | **AUC** |
|---|---|
| Coudray et al. [4] | 0.85 |
| Khosravi et al. [20] | 0.83 |
| Yu et al. [31] | 0.75 |
| **Proposed method** | **0.89** |

Table 2: Performance of various methods for LUAD/LUSC predictions using transfer learning. Our results report the average of 5-fold accuracy values.

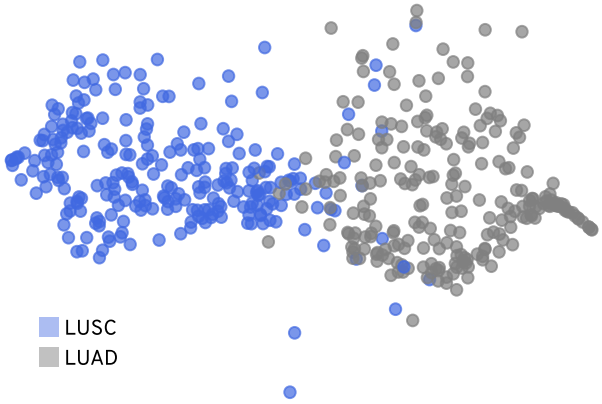


Figure 4: t-SNE visualization of feature vectors extracted after the Graph Pooling layer from different WSIs. The two distinct clusters for LUAD and LUSC demonstrate the efficacy of the proposed model for disease characterization in WSIs. The overlap of two clusters contain WSIs that are morphologically and visually similar.

**Inference.** One of the primary obstacles for real-world application of deep learning models in computer-aided diagnosis is the black-box nature of the deep neural networks. Since our proposed architecture uses Global Attention Pooling [22], we can visualize the importance that our network gives to each patch for making the final prediction. Such visualization can provide more insight to pathologists regarding the model's internal decision making. The global attention pooling layer learns to map patches to "attention" values. The higher attention values signify that the model focuses more on those patches. We visualize the patches with high and low attention values in Figure 3. One of the practical applications of our approach would be for triaging. As new cases are queued for an expert's analysis, the CAD system could highlight the regions of interests and sort the cases based on the diagnostic urgency. We observe that patches with higher attention values generally contain more nuclei. As morphological features of nuclei are vitals for making diagnostic decisions [25], it is interesting to note this property is learned on its own by the network. Figure 4 shows the t-SNE plot of features vectors for some of the WSIs. It shows the clear distinction between the two cancer subtypes, further favoring the robustness of our method.

**Implementation Details.** We used PyTorch Geometric library to implement graph convolution networks [8]. We

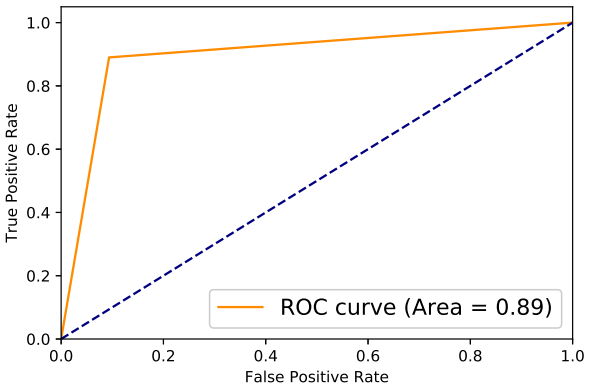


Figure 5: The ROC curve of prediction.

used pre-trained DenseNet [14] to extract features from histopathology patches. We further feed DenseNet features through three dense layers with dropout ($p = 0.5$).

**Ablation Study.** We tested our method with various different configurations for the TCGA dataset. We used two layers in Graph Convolution Network—ChebNet and SAGE Convolution. We found that ChebNet outperforms SAGE Convolution and also results in better generalization. Furthermore, we experimented with different numbers of filters in ChebNet, and also different pooling layers—global attention, mean, max, and sum pooling. We feed the pooled representation to two fully connected Dense layers to get the final classification between LUAD and LUSC. All the different permutations of various parameters result in 32 different configurations, the results for all these configurations are provided in Table 3. It should be noted that the results reported in the previous sections are based on Cheb-7 with mean pooling.

## 6. Conclusion

The accelerated adoption of digital pathology is coinciding with and probably partly attributed to recent progress in AI applications in the field of pathology. This disruption in the field of pathology offers a historic chance to find novel solutions for major challenges in diagnostic histopathology and adjacent fields, including biodiscovery. In this study, we proposed a technique for representing an entire WSI as a fully-connected graph. We used the graph convolution networks to extract the features for classifying the lung WSIs into LUAD or LUSC. The results show the good performance of the proposed approach. Furthermore, the proposed method is explainable and transparent as we can use attention values and adjacency matrix to visualize relevant patches.

## References


[1] Deepak Anand, Shrey Gadiya, and Amit Sethi. Histographs: graphs in histopathology. In *Medical Imaging 2020: Digital Pathology*, volume 11320, page 113200O. International Society for Optics and Photonics, 2020. 2

[2] Jocelyn Barker, Assaf Hoogi, Adrien Depeursinge, and Daniel L Rubin. Automated classification of brain tumor type in whole-slide digital pathology images using local representative tiles. *Medical image analysis*, 30:60–71, 2016. 2

[3] Marc-André Carbonneau, Veronika Cheplygina, Eric Granger, and Ghyslain Gagnon. Multiple instance learning: A survey of problem characteristics and applications. *Pattern Recognition*, 77:329–353, 2018. 2

[4] Nicolas Coudray, Paolo Santiago Ocampo, Theodore Sakellaropoulos, Navneet Narula, Matija Snuderl, David Fenyö, Andre L Moreira, Narges Razavian, and Aristotelis Tsirigos. Classification and mutation prediction from non–small cell lung cancer histopathology images using deep learning. *Nature medicine*, 24(10):1559–1567, 2018. 6

[5] Michaël Defferrard, Xavier Bresson, and Pierre Vandergheynst. Convolutional neural networks on graphs with fast localized spectral filtering. In *Advances in neural information processing systems*, pages 3844–3852, 2016. 3

[6] Neofytos Dimitriou, Ognjen Arandjelović, and Peter D Caie. Deep learning for whole slide image analysis: An overview. *Frontiers in Medicine*, 6, 2019. 2

[7] Dheeru Dua and Casey Graff. UCI machine learning repository, 2017. 5

[8] Matthias Fey and Jan E. Lenssen. Fast graph representation learning with PyTorch Geometric. In *ICLR Workshop on Representation Learning on Graphs and Manifolds*, 2019. 6

[9] Simon Graham, Muhammad Shaban, Talha Qaiser, Navid Alemi Koohbanani, Syed Ali Khurram, and Nasir Rajpoot. Classification of lung cancer histology images using patch-level summary statistics. In *Medical Imaging 2018: Digital Pathology*, volume 10581, page 1058119. International Society for Optics and Photonics, 2018. 5

[10] Metin N. Gurcan, Laura Boucheron, Ali Can, Anant Madabhushi, Nasir Rajpoot, and Bulent Yener. Histopathological Image Analysis: A Review. 2:147–171, 2009. 2

[11] David A Gutman, Jake Cobb, Dhananjaya Somanna, Yuna Park, Fusheng Wang, Tahsin Kurc, Joel H Saltz, Daniel J Brat, Lee AD Cooper, and Jun Kong. Cancer digital slide archive: an informatics resource to support integrated in silico analysis of tcga pathology data. *Journal of the American Medical Informatics Association*, 20(6):1091–1098, 2013. 2, 5

[12] Will Hamilton, Zhitao Ying, and Jure Leskovec. Inductive representation learning on large graphs. In *Advances in neural information processing systems*, pages 1024–1034, 2017. 3

[13] David K Hammond, Pierre Vandergheynst, and Rémi Gribonval. Wavelets on graphs via spectral graph theory. *Applied and Computational Harmonic Analysis*, 30(2):129–150, 2011. 3

| configuration | **mean** | attention | max | add |
|---|---|---|---|---|
| **Cheb-7** | **0.8889** | 0.8853 | 0.7891 | 0.4929 |
| Cheb 3_BN | 0.8771 | 0.8635 | 0.8471 | 0.5018 |
| Cheb 5 | 0.8762 | 0.8830 | 0.8750 | 0.5082 |
| Cheb 3 | 0.8752 | 0.8735 | 0.8702 | 0.5090 |
| Cheb 5_BN | 0.8596 | 0.8542 | 0.7179 | 0.4707 |
| Cheb 7_BN | 0.7239 | 0.6306 | 0.5618 | 0.4930 |
| SAGE CONV_BN | 0.6866 | 0.5848 | 0.6281 | 0.5787 |
| SAGE CONV | 0.5784 | 0.6489 | 0.5389 | 0.5690 |

Table 3: Comparison of different network architecture and pooling method (attention, mean, max and sum pooling). **BN** stands for BatchNormalization [17], **Cheb** stands for Chebnet with corresponding filter size and **SAGE** stands for SAGE Convolution. The best performing configuration is Cheb-7 with mean pooling.


[14] Gao Huang, Zhuang Liu, Laurens Van Der Maaten, and Kilian Q Weinberger. Densely connected convolutional networks. In *Proceedings of the IEEE conference on computer vision and pattern recognition*, pages 4700–4708, 2017. 3, 5, 7

[15] Maximilian Ilse, Jakub M Tomczak, and Max Welling. Attention-based deep multiple instance learning. *arXiv preprint arXiv:1802.04712*, 2018. 2, 5

[16] Maximilian Ilse, Jakub M Tomczak, and Max Welling. Deep multiple instance learning for digital histopathology. In *Handbook of Medical Image Computing and Computer Assisted Intervention*, pages 521–546. Elsevier, 2020. 2

[17] Sergey Ioffe and Christian Szegedy. Batch normalization: Accelerating deep network training by reducing internal covariate shift. *arXiv preprint arXiv:1502.03167*, 2015. 8

[18] S Kalra, C Choi, S Shah, L Pantanowitz, and HR Tizhoosh. Yottixel–an image search engine for large archives of histopathology whole slide images. *arXiv preprint arXiv:1911.08748*, 2019. 3, 5

[19] Shivam Kalra, HR Tizhoosh, Sultaan Shah, Charles Choi, Savvas Damaskinos, Amir Safarpoor, Sobhan Shafiei, Morteza Babaie, Phedias Diamandis, Clinton JV Campbell, et al. Pan-cancer diagnostic consensus through searching archival histopathology images using artificial intelligence. *npj Digital Medicine*, 3(1):1–15, 2020. 5

[20] Pegah Khosravi, Ehsan Kazemi, Marcin Imielinski, Olivier Elemento, and Iman Hajirasouliha. Deep convolutional neural networks enable discrimination of heterogeneous digital pathology images. *EBioMedicine*, 27:317–328, 2018. 6

[21] Daisuke Komura and Shumpei Ishikawa. Machine learning methods for histopathological image analysis. *Computational and Structural Biotechnology Journal*, 2018. 2

[22] Yujia Li, Daniel Tarlow, Marc Brockschmidt, and Richard Zemel. Gated graph sequence neural networks. *arXiv preprint arXiv:1511.05493*, 2015. 3, 6

[23] Anant Madabhushi, Shannon Agner, Ajay Basavanhally, Scott Doyle, and George Lee. Computer-aided prognosis: Predicting patient and disease outcome via quantitative fusion of multi-scale, multi-modal data. 35(7):506–514, 2011. 2

[24] Anant Madabhushi and George Lee. Image analysis and machine learning in digital pathology: Challenges and opportunities. *Medical Image Analysis*, 33:170–175, oct 2016. 2

[25] Shivang Naik, Scott Doyle, Shannon Agner, Anant Madabhushi, Michael Feldman, and John Tomaszewski. Automated gland and nuclei segmentation for grading of prostate and breast cancer histopathology. In *2008 5th IEEE International Symposium on Biomedical Imaging: From Nano to Macro*, pages 284–287. IEEE, 2008. 6

[26] PJ Sudharshan, Caroline Petitjean, Fabio Spanhol, Luiz Eduardo Oliveira, Laurent Heutte, and Paul Honeine. Multiple instance learning for histopathological breast cancer image classification. *Expert Systems with Applications*, 117:103–111, 2019. 2

[27] Jakub M Tomczak, Maximilian Ilse, and Max Welling. Deep learning with permutation-invariant operator for multi-instance histopathology classification. *arXiv preprint arXiv:1712.00310*, 2017. 2

[28] Ming Tu, Jing Huang, Xiaodong He, and Bowen Zhou. Multiple instance learning with graph neural networks. *arXiv preprint arXiv:1906.04881*, 2019. 2, 4, 5

[29] Xinggang Wang, Yongluan Yan, Peng Tang, Xiang Bai, and Wenyu Liu. Revisiting multiple instance neural networks. *Pattern Recognition*, 74:15–24, 2018. 5

[30] John N Weinstein, Eric A Collisson, Gordon B Mills, Kenna R Mills Shaw, Brad A Ozenberger, Kyle Ellrott, Ilya Shmulevich, Chris Sander, Joshua M Stuart, Cancer Genome Atlas Research Network, et al. The cancer genome atlas pan-cancer analysis project. *Nature genetics*, 45(10):1113, 2013. 2

[31] Kun-Hsing Yu, Ce Zhang, Gerald J Berry, Russ B Altman, Christopher Ré, Daniel L Rubin, and Michael Snyder. Predicting non-small cell lung cancer prognosis by fully automated microscopic pathology image features. *Nature communications*, 7:12474, 2016. 6

[32] Manzil Zaheer, Satwik Kottur, Siamak Ravanbakhsh, Barnabas Poczos, Russ R Salakhutdinov, and Alexander J Smola. Deep sets. In *Advances in neural information processing systems*, pages 3391–3401, 2017. 3, 4

[33] Zhi-Hua Zhou, Yu-Yin Sun, and Yu-Feng Li. Multi-instance learning by treating instances as non-iid samples. In *Proceedings of the 26th annual international conference on machine learning*, pages 1249–1256, 2009. 5